Since January 2020 Elsevier has created a COVID-19 resource centre with free information in English and Mandarin on the novel coronavirus COVID-19. The COVID-19 resource centre is hosted on Elsevier Connect, the company's public news and information website.

Cell Reports

CRISPR-Csy4-Mediated Editing of Rotavirus Double-Stranded RNA Genome

Graphical Abstract

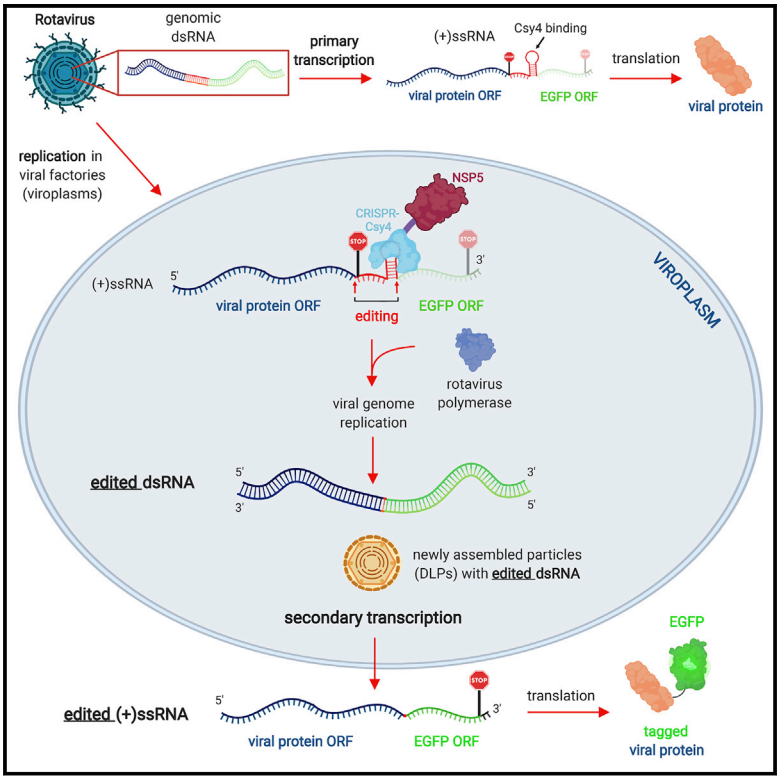

Highlights

- CRISPR-Csy4 fused with NSP5 can cleave rotavirus (+) ssRNA inside viroplasms
- Csy4-cleaved (+)ssRNA replication intermediates are repaired as edited viral dsRNA
- Csy4 editing allows detection of products of secondary transcription
- Secondary transcription is the main source of rotavirus proteins in infected cells

Authors

Guido Papa, Luca Venditti, Luca Braga, Edoardo Schneider, Mauro Giacca, Gianluca Petris, Oscar R. Burrone

Correspondence

gpapa@mrc-lmb.cam.ac.uk (G.P.), gpetris@mrc-lmb.cam.ac.uk (G.P.), burrone@icgeb.org (O.R.B.)

In Brief

Papa et al. engineer the CRISPR-Csy4 nuclease to localize into rotavirus viral factories and cleave (+)ssRNA replication intermediates, producing edits of the targeted dsRNA genome segment. This allows for the detection of secondary transcription-derived proteins made by the newly assembled viruses, demonstrating that they largely contribute to overall viral protein production.

Papa et al., 2020, Cell Reports *32*, 108205
September 29, 2020
https://doi.org/10.1016/j.celrep.2020.108205

CellPress

Cell Reports

CellPress
OPEN ACCESS

Report

CRISPR-Csy4-Mediated Editing of Rotavirus Double-Stranded RNA Genome

Guido Papa,[1,5,*] Luca Venditti,[1] Luca Braga,[2,3] Edoardo Schneider,[2,3] Mauro Giacca,[2,3] Gianluca Petris,[4,*] and Oscar R. Burrone[1,6,*]

[1]Molecular Immunology Laboratory, International Centre for Genetic Engineering and Biotechnology (ICGEB), Padriciano 99, 34149 Trieste, Italy

[2]Molecular Medicine Laboratory, International Centre for Genetic Engineering and Biotechnology (ICGEB), Padriciano 99, 34149 Trieste, Italy

[3]British Heart Foundation Centre of Research Excellence, School of Cardiovascular Medicine & Sciences, King's College London, London, UK

[4]Medical Research Council Laboratory of Molecular Biology (MRC LMB), Cambridge Biomedical Campus, Francis Crick Avenue, Cambridge CB2 0QH, UK

[5]Present address: Medical Research Council Laboratory of Molecular Biology (MRC LMB), Cambridge Biomedical Campus, Francis Crick Avenue, Cambridge CB2 0QH, UK

[6]Lead Contact

*Correspondence: gpapa@mrc-lmb.cam.ac.uk (G.P.), gpetris@mrc-lmb.cam.ac.uk (G.P.), burrone@icgeb.org (O.R.B.)

https://doi.org/10.1016/j.celrep.2020.108205

SUMMARY

CRISPR-nucleases have been widely applied for editing cellular and viral genomes, but nuclease-mediated genome editing of double-stranded RNA (dsRNA) viruses has not yet been reported. Here, by engineering CRISPR-Csy4 nuclease to localize to rotavirus viral factories, we achieve the nuclease-mediated genome editing of rotavirus, an important human and livestock pathogen with a multisegmented dsRNA genome. Rotavirus replication intermediates cleaved by Csy4 is edited through the formation of precise deletions in the targeted genome segments in a single replication cycle. Using CRISPR-Csy4-mediated editing of rotavirus genome, we label the products of rotavirus secondary transcription made by newly assembled viral particles during rotavirus replication, demonstrating that this step largely contributes to the overall production of viral proteins. We anticipate that the nuclease-mediated cleavage of dsRNA virus genomes will promote an advanced level of understanding of viral replication and host-pathogen interactions, also offering opportunities to develop therapeutics.

INTRODUCTION

Prokaryotes have evolved an anti-viral defense mechanism based on CRISPR loci. These regions express pre-CRISPR RNAs (pre-crRNAs) containing short virus-derived sequences. These transcripts are processed to generate crRNAs, which are used to guide CRISPR nucleases to cleave foreign nucleic acids (Jinek et al., 2012). The six known types of CRISPR-Cas systems have different mechanisms of crRNA maturation (Makarova et al., 2018).

The CRISPR-Cas type I and type III (and likely type IV) systems use an endoribonuclease of the Cas6 superfamily to cleave an invariant portion of the pre-crRNAs to generate the mature crRNAs (Murugan et al., 2017; Özcan et al., 2019). Among them, Csy4/Cas6f of *Pseudomonas aeruginosa* type I-F CRISPR systems (Makarova et al., 2018), is a well-characterized small (21 kDa) and highly specific single-turnover RNA endoribonuclease, processing pre-crRNAs in a 28-nucleotide (nt) sequence (Cy28) to generate the mature crRNAs. Csy4 specifically binds a 16-nt RNA hairpin within Cy28 with very high affinity (KD = 50 pM) and cleaves directly downstream of the five-base-pair stem element (Haurwitz et al., 2010; Sternberg et al., 2012; Lee et al., 2013). Csy4 has already been applied to cleave several engineered Cy28-containing RNAs for biotechnological applications including a model human immunodeficiency virus (HIV) (Guo et al., 2015; Nissim et al., 2014; Lee et al., 2013).

Here, we applied Csy4 to rotavirus (RV), an important animal and human pathogen of the Reoviridae family with a multisegmented double-stranded (dsRNA) genome, which replicates in cytoplasmic viral factories named viroplasms (Desselberger, 2014; Eichwald et al., 2004). Protein access to viroplasms is mainly restricted to some viral proteins and is regulated in a still unrecognized way (Eichwald et al., 2012). Exogenous non-viral proteins and exogenous viral RNAs are usually confined outside viroplasms (Campagna et al., 2005; Silvestri et al., 2004). In the past, we succeeded to localize EGFP and mCherry into viroplasms by fusing them to either of the RV non-structural proteins NSP5 or NSP2 (Eichwald et al., 2004; Papa et al., 2019). Here, we used these two viral proteins to shuttle CRISPR-Csy4 nuclease to RV viroplasms and to obtain the nuclease-mediated site-specific genome editing of a dsRNA virus. Using different recombinant RVs (rRVs) carrying the Csy4 target sequence in diverse positions and viral segments, we report that nuclease cleavage of viral positive single-stranded RNA ((+)ssRNA) within viroplasms results in small sequence-dependent deletions of the targeted genomic segment (gs) in a single replication cycle.

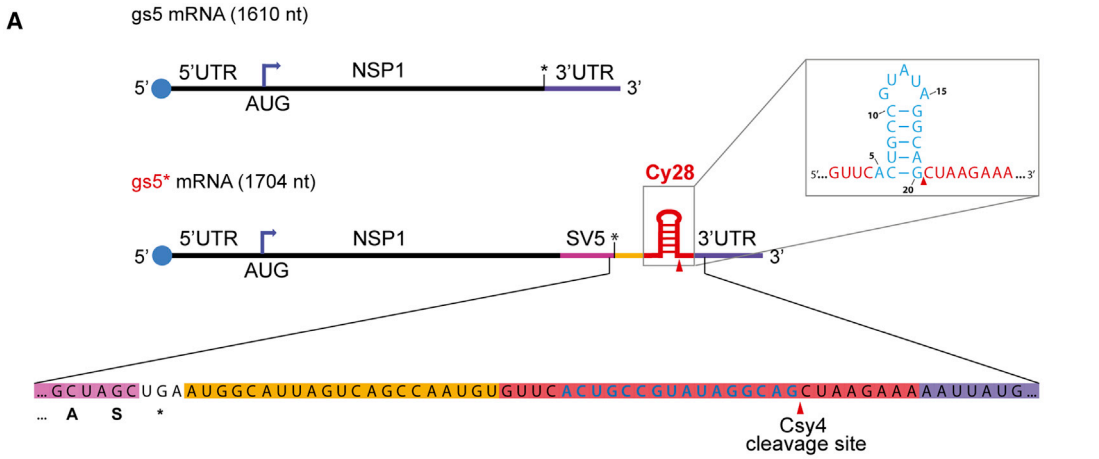

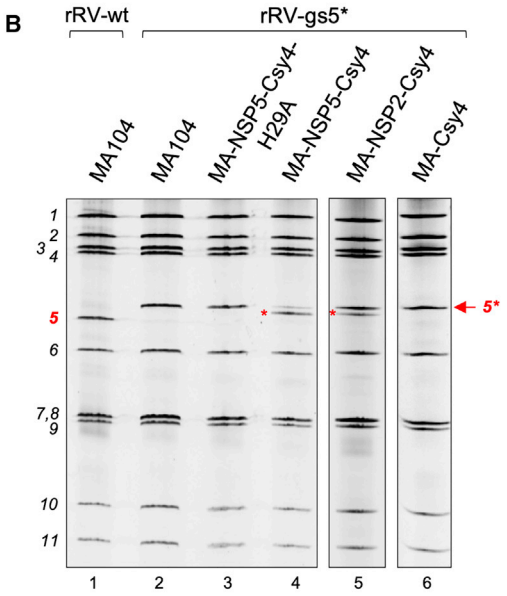

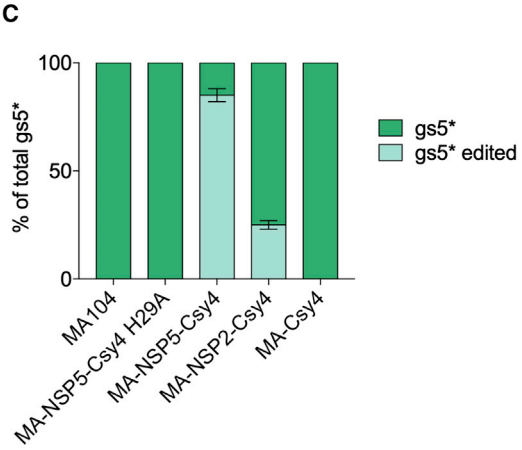

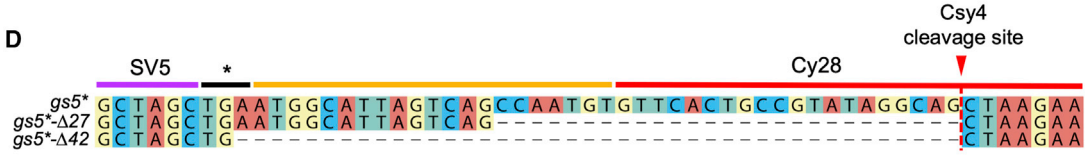

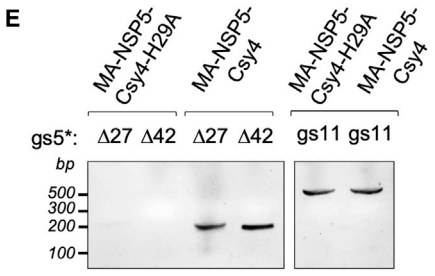

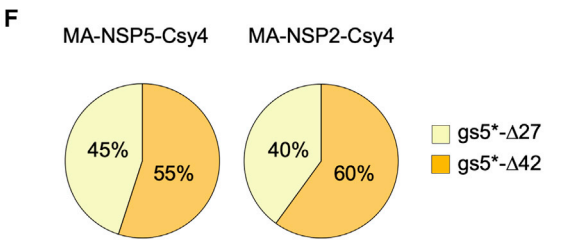

(legend on next page)

Using RV genome editing, we labeled products of RV secondary transcription, demonstrating the main role of secondary transcription in the overall production of viral proteins.

RESULTS

Targeting CRISPR-Csy4 to RV Viroplasms

To investigate the effect of Csy4 cleavage of rRV (+)ssRNAs, we first generated different SV5-tagged Csy4 stable MA104 cell lines. MA104 cells are widely used to study RV replication (Wu et al., 2017). Csy4 was expressed at lower levels (MA-Csy4) than Csy4-H29A (MA-Csy4-H29A) (Figure S1A), a catalytically inactive variant that preserves strong substrate binding affinity (Haurwitz et al., 2010; Sternberg et al., 2012). Csy4-H29A showed diffuse cytoplasmic distribution with no viroplasm localization in rRV-infected cells (Figure S1B). As RV NSP5 and NSP2 localize to viroplasms (Eichwald et al., 2004), we fused them to SV5-tagged Csy4 or Csy4-H29A to generate the MA104 cell lines named MA-NSP5-Csy4, MA-NSP2-Csy4, and MA-NSP5-Csy4-H29A (Figure S1C). Both NSP5-Csy4 and NSP5-Csy4-H29A fusion proteins showed higher expression than the NSP2-Csy4 chimera (Figure S1C). All three fusion proteins localized to viroplasms upon RV infection, whereas they showed a diffuse cytoplasmic distribution in non-infected cells (Figures S1D–S1F). In MA-NSP5-Csy4 and MA-NSP5-Csy4-H29A cells, the number and size of viroplasms, the production of viral proteins (VP2 and NSP5), and viral progeny yield did not differ from those of parental MA104 cells (Figures S2A–S2D).

Activity of Csy4 and Csy4 Fusion Variants

RNA cleavage activity of the Csy4 variants was evaluated using an EGFP reporter plasmid having the Cy28 target sequence located immediately after the ATG initiation codon (Figure S2E), and the cleavage of the reporter transcript was measured as reduction of EGFP fluorescence (Borchardt et al., 2015). In MA-NSP5-Csy4 cells, EGFP expression was abolished (a 20-fold decrease) compared to cells expressing the Csy4-H29A mutant and the parental MA104 (Figure S2E), and a 4-fold decrease in EGFP fluorescence was observed in MA-NSP2-Csy4 and MA-Csy4 cells (Figure S2E). Expression levels of control EGFP lacking the Cy28 target sequence showed no differences among all the samples (Figure S2F). These data indicate that NSP2/NSP5-Csy4 fusion constructs represent an ideal tool to evaluate the effect of Csy4 nuclease activity on RV replication.

Viroplasm-Targeted Csy4 Nuclease Mediates Editing of RV gs5

The RV genome segment 5 (gs5) includes a single open reading frame (ORF) expressing the 60-kDa non-structural protein NSP1, which antagonizes the interferon response (Barro and Patton, 2007; Davis and Patton, 2017) but is dispensable for virus replication in cultured cells (Kanai et al., 2017; Komoto et al., 2018). We used the recently developed fully tractable RV reverse genetics system (Komoto et al., 2018; Papa et al., 2019) to generate a rRV (SA11 strain) containing a modified gs5 (rRV-gs5*). The engineered gs5* encoded NSP1 C-terminally tagged with SV5 and had the Cy28 sequence in the (+)ssRNA strand between the STOP codon and the 3′ untranslated region (3′ UTR) (Figure 1A). The genomic dsRNA migration profile of rRV-gs5* showed the expected increase in size of gs5 (gs5*, red arrow), also confirmed by sequencing, and packaging of all the other genome segments (Figures S3A and S3D). rRV-gs5*-infected MA104 cells produced the 60-kDa SV5-tagged NSP1 protein and similar hyperphosphorylation of the RV essential protein NSP5 (Figure S3B; Eichwald et al., 2004; Papa et al., 2019). rRV-gs5* showed minimal changes in viral replication at early hours post-infection (hpi) compared to rRV-wild type (rRV-WT), even though a slightly reduced replication fitness was present at late hpi (Figure S3C).

rRV-gs5* was designed to investigate the fate of virus replication upon cleavage of the (+)ssRNA transcript by Csy4 chimeras. At 16 hpi in MA-NSP5-Csy4 cells, the newly produced rRV-gs5* dsRNAs showed that 80% of gs5* migrated as a shorter segment (Figures 1B and 1C) and further passages resulted in complete gs5* editing (Figures S3E and S3F). In contrast, infection of the parental MA104 or MA-NSP5-Csy4-H29A did not show any difference in the dsRNA migration patterns (Figures 1B and 1C). The gs5* deletion was less frequent (20% of the total gs5*) in MA-NSP2-Csy4 cells (Figures 1B and 1C), consistently with their lower Csy4 activity (Figure S2E). Genome editing of gs5* dsRNA required Csy4 localization to viroplasms, as infection of MA-Csy4 cells, with the nuclease not targeted to viroplasms, did not affect the migration pattern of the newly made gs5* (Figures 1B and 1C). These data suggest that RV genome editing requires cleavage of the (+)ssRNA, which is used as the template of the replication intermediates within viroplasms (Silvestri et al., 2004). Finding the edited gs5* was remarkable, not only because it showed that nuclease-mediated cleavage of RV genome replication intermediates can be repaired but also for the very high efficiency and because, in RV, spontaneous genome modifications have been mainly described as partial duplications (Desselberger, 1996; Giambiagi et al., 1994; González et al., 1989; Méndez et al., 1992; Schnepf et al., 2008; Troupin et al., 2011). Sequence analysis of the edited gs5* revealed that it consisted of a mixture of two segments carrying a deletion of either 42 (gs5*-Δ42) or 27 nt (gs5*-Δ27) compared to gs5* (Figure 1D), which was detected also by transcript-specific reverse-transcriptase PCR (RT-PCR) at 7 hpi (Figure 1E). The two different Csy4 viral shuttle proteins (NSP5 and NSP2) produced similar

Figure 1. CRISPR-Csy4 Editing of rRV gs5

(A) Scheme of (+)ssRNA of WT gs5 and gs5*, whose sequence is shown below; red arrowhead indicates Csy4 cleavage site. The 16-nt Csy4 binding site in Cy28 is highlighted in blue.

(B and C) Electrophoretic pattern (B) and quantification (C) of dsRNA genome of rRV-WT or rRV-gs5* derived from indicated cells at 16 hpi. Red arrow, gs5*; red asterisks, edited gs5*. Genomic segments are indicated on the left. For (C), data are means ± SEM.

(D) Sequence of edited gs5*-Δ27 and gs5*-Δ42.

(E) RT-PCR products of gs5*-Δ27 (174 bp) and gs5*-Δ42 (159 bp) and gs11 (as control) from rRV-gs5*-infected cells at 7 hpi.

(F) Relative frequencies of gs5*-Δ27 and gs5*-Δ42 (45 clones for MA-NSP5-Csy4 and 30 clones for MA-NSP2-Csy4).

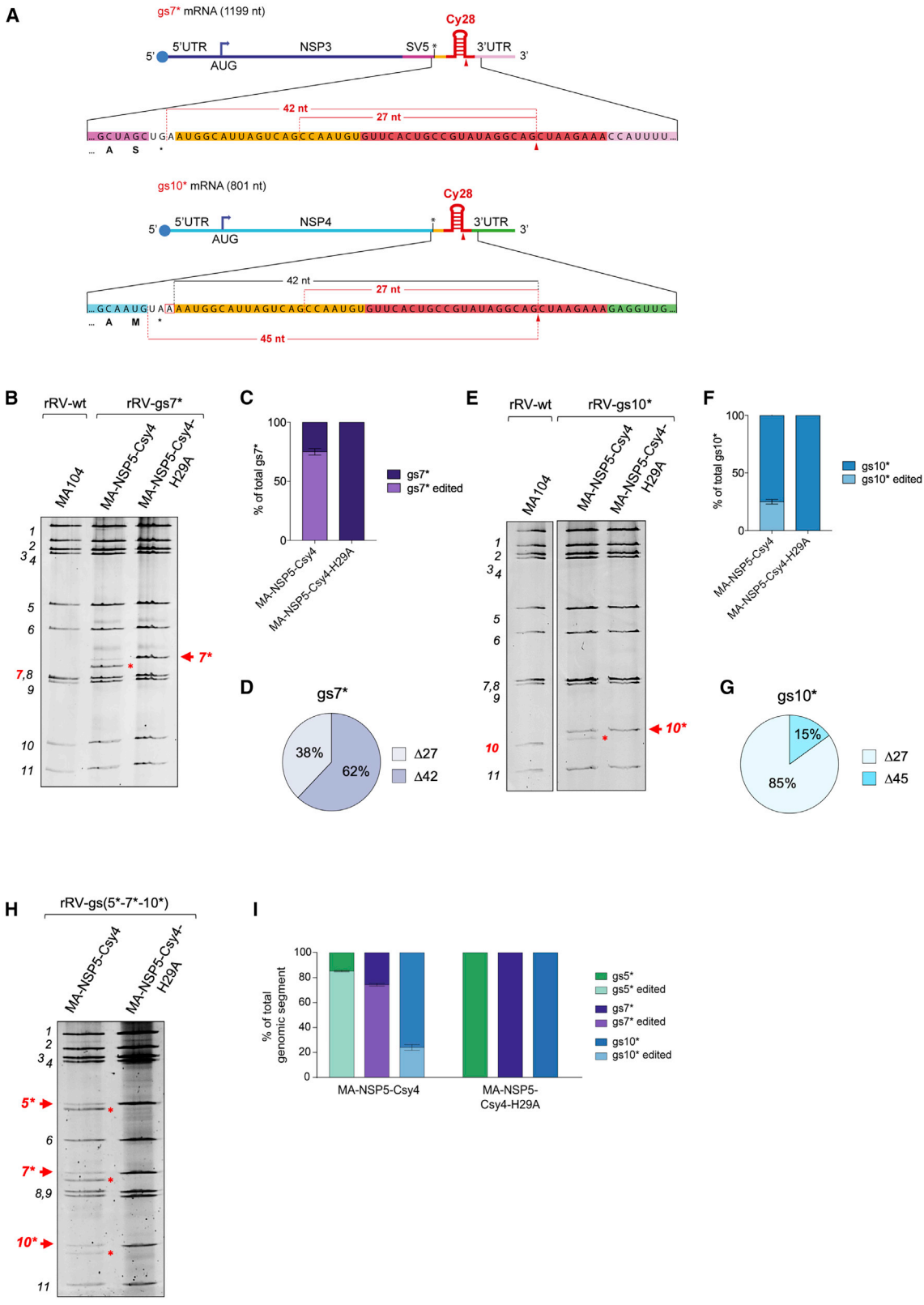

(legend on next page)

gs5* editing outcomes, with the Δ42 deletion slightly more frequent (55% NSP5-Csy4, 60% NSP2-Csy4) than the Δ27 (45% NSP5-Csy4, 40% NSP2-Csy4) (Figure 1F).

The 3′ end of both deletions was always compatible with the Csy4 cleavage site (Figure 1D), consistent with Csy4 nuclease activity. In both cases, a G nucleotide was present immediately upstream of the deletions. The two newly edited rRVs gs5*-Δ42 and gs5*-Δ27 were independently packaged into newly made viral particles and were not further mutated after 6 consecutive passages in MA104 cells, as confirmed by sequencing (Figures S3H and S3I). Consistent with the Csy4 high specificity (Haurwitz et al., 2012, 2010; Sternberg et al., 2012; Lee et al., 2013), deletions were observed exclusively in the rRV gs5* containing the Csy4 target sequence (Figure 1B; Figure S3H) and rRV-WT equally replicated in cells with active or inactive Csy4 fusions, suggesting a lack of Csy4 off-target editing of rRV-WT double-stranded genome segments (Figure S3G).

To investigate whether gs5* editing was dependent on the position of the nuclease target sequence, we generated rRV-gs5*/284 carrying, similarly to gs5*, the same Cy28 sequence located in this case 284 nts (instead of 95) upstream of the 3′ end (Figure S4A). As NSP1 is dispensable for viral replication in RV-infected cells (Komoto et al., 2018), NSP1 truncation did not affect rescue of the rRV-gs5*/284.

The dsRNA profile and sequencing showed that 95% of gs5*/284 was edited in MA-NSP5-Csy4 cells but not in parental MA104 or MA-NSP5-Csy4-H29A cells (Figures S4B and S4C). The edited gs5*/284 segments contained, with similar frequency, the same Δ42 (66%) and Δ27 (34%) deletions observed for gs5* (Figure S4D); these findings ruled out that the Cy28 position affects the editing outcome.

CRISPR-Csy4 Editing of RV gs7 and gs10 and Multiplex Editing

To investigate editing events in other genome segments, we first obtained a rRV with a modified gs7 (rRV-gs7*), in which NSP3 was C-terminally SV5 tagged and the Cy28 sequence inserted after the UGA STOP codon (Figure 2A, top panel). Upon infection of MA-NSP5-Csy4 cells, 80% of gs7* was edited, whereas no modifications were observed in other RV gss or in cells expressing NSP5-Csy4-H29A (Figures 2B and 2C). The same Δ27 and Δ42 deletions (38% and 62%, respectively) (Figure 2D) as observed in gs5* and gs5*/284 were generated, suggesting that the editing outcome was dependent of the inserted sequence, which was identical in all three recombinant gss (Figures 1A and 2A).

We then targeted Csy4 to gs10 that encodes NSP4. The rRV-gs10* was thus generated, containing the same Cy28 sequence placed after the natural NSP4 UAA STOP codon (Figure 2A, bottom panel). The different STOP codon used removed the G previously involved in the formation of the modal Δ42 editing detected in gs5*, gs5*/284, and gs7*. Upon infection of MA-NSP5-Csy4, but not MA-NSP5-Csy4-H29A cells, a band of edited gs10* was detected and represented 20% of total gs10* (Figures 2E and 2F). We observed the same Δ27 editing event (85%) and a new deletion (Δ45) of 45 nt (15%), which also involved a G nucleotide (Figure 2G). The absence of the Δ42 editing and the appearance of the Δ45 suggest that the G upstream of the deletion plays an important role in determining the editing outcome. This finding was further confirmed in gs5 with a new rRV (rRV-gs5*-GA) having the G (at −28 nt from Csy4 cleavage site) involved in the Δ27 deletion mutated into A (Figure S4E). In MA-NSP5-Csy4 cells, gs5*-GA was edited only to the Δ42 deletion and the Δ27 editing was not detected (Figures S4F–S4H).

To test Csy4 for multiplexed RV genome editing, we generated rRV-gs(5*-7*-10*), with the Cy28 sequence present in three different RV genome segments (gs5*, gs7*, and gs10*). Upon infection of MA-NSP5-Csy4, but not MA-NSP5-Csy4-H29A cells, all three genome segments were edited in a similar proportion and with the same deletions as in viruses in which only a single genome segment was targeted (Figures 2H and 2I; Figures S5A and S5B). Migration of other segments was unaffected. These data indicate that the Csy4 cleavage of RV (+)ssRNA templates within viroplasms can be exploited to generate simultaneous precise editing events in multiple genome segments in a single replication cycle.

Csy4-Mediated Editing to Study RV Secondary Transcription

A hallmark of RV biology is the transcriptional activity of intermediate viral particles (Desselberger, 2014). Mature RVs are triple layered particles (TLPs) that after entry lose the outer layer and become transcriptionally active double layered particles (DLPs). DLPs generate transcripts used as templates for the dsRNA synthesis and as mRNAs to produce viral proteins. During virus replication, newly made DLPs are assembled within viroplasms and are supposed to start a new wave of transcription called secondary transcription before budding into the endoplasmic reticulum (ER) and maturing into TLPs (Estes and Greenberg, 2013).

To what degree secondary transcription and the consequent translation contribute to the overall production of viral proteins remains unknown (López et al., 2005). Csy4 editing of the RV genome is an approach to study secondary transcription by monitoring the expression of edited genome segments in a single replication cycle. Upon transcription, the newly generated edited segments produce mRNAs different from the one of the original infective particles.

To detect proteins produced exclusively by edited mRNA, we engineered rRV-gs5*-HA, containing a short 23-nt Csy4 target

Figure 2. Single and Multiplexed Csy4-Mediated Editing of gs5, gs7, and gs10

(A) Scheme of gs7* (top panel) and gs10* (bottom panel) (+)ssRNAs. Detected deletions are indicated in red.

(B) dsRNA electropherotypes of rRV-gs7* infecting the indicated cells at 16 hpi.

(C) Quantification of gs7* editing; data are means ± SEM (n = 3).

(D–I) Relative proportion of each edited gs7* sequence (40 clones) (D). (E), (F), and (G) are as in (B), (C), and (D) in cells infected with rRV-gs10*. (H) and (I) are as in (B) and (C) in cells infected with rRV-gs(5*-7*-10*). Data are means ± SEM (n = 2). In all panels, red arrows indicate gs5*, gs7*, or gs10*; red asterisks indicate their edited versions.

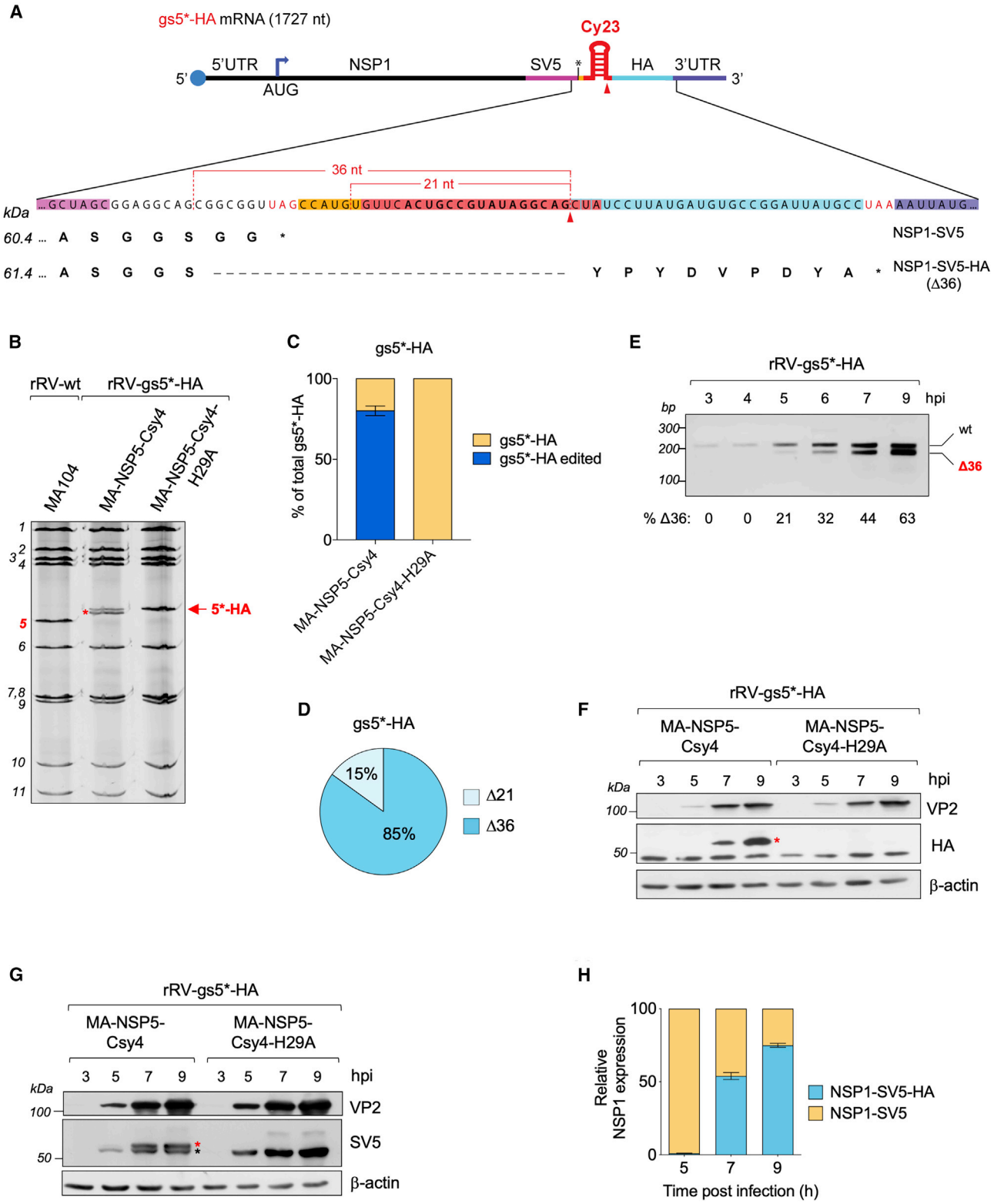

Figure 3. Csy4-Mediated Detection of Secondary Transcription

(A) Scheme of gs5*-HA (+)ssRNA, showing the in-frame Δ36 deletion producing NSP1-HA and the Δ21 deletion. C-terminal amino acid sequence and expected molecular masses of NSP1-SV5 and NSP1-SV5-HA are shown. Arrowhead indicates the Csy4 cleavage site.

(legend continued on next page)

sequence (Cy23) (Sternberg et al., 2012), and the hemagglutinin (HA)-tag coding sequence downstream of the NSP1-SV5 STOP codon (Figure 3A). gs5*-HA was designed to express HA-tagged isoforms of NSP1-SV5 after in-frame deletions of at least 27 nts, which eliminate the STOP codon (Figure 3A). In MA-NSP5-Csy4 cells, rRV-gs5*-HA was edited to 36- and 21-nt deletions, with a total editing efficiency of 80% at 16 hpi (Figures 3B–3D). The gs5*-HA Δ36 transcript was detected from 5 hpi and became more abundant (63% versus 36%) than the non-edited gs5*-HA at 9 hpi (Figure 3E). The Δ36 editing was expected to result in a 61.4-kDa HA-tagged NSP1-SV5 protein, whereas the Δ21 and the non-edited gs5*-HA encoded a 60.4-kDa NSP1-SV5 isoform (Figure 3A). Western blot analysis detected the HA-tagged NSP1-SV5 in MA-NSP5-Csy4 cells from 7 hpi (Figure 3F) but not in MA-NSP5-Csy4-H29A cells, in which gs5*-HA was not edited (Figures 3B, 3C, and 3F). As only newly made particles can contain an edited gs5*-HA, expression of NSP1-SV5-HA allowed monitoring translation of the newly produced transcripts derived from secondary transcription. Time course analysis using an anti-SV5 antibody, which recognizes both HA-edited and non-edited NSP1, showed that from 5 to 9 hpi, production of NSP1-SV5-HA progressively increased, becoming predominant (73%) at 9 hpi (Figures 3G and 3H). The contribution of the secondary transcription is likely underestimated because of the incomplete editing of gs5*-HA and the generation of the not HA-labeled Δ21 isoform. Encouraged by this result, we produced rRV-gs5*-HA-EGFP* (Figure 4A), which would express EGFP only upon Csy4-mediated in-frame deletion of at least 27 nts in the engineered gs5. The two G nucleotides upstream Cy23 involved in the formation of the Δ21 and Δ27 deletions were mutated to A. The size of gs5*-HA-EGFP* was too large to detect the edited segment by dsRNA gel migration (Figure S6A), but by Sanger sequencing decomposition (Brinkman et al., 2014), the total editing efficiency was 9.6% and the only significant editing event was the in-frame Δ36 deletion (Figure S6B). Cytofluorimetric analysis (Figure 4B) and confocal fluorescence images (Figures 4C and 4D; Figure S6C) of NSP1-EGFP spots (Murphy and Arnold, 2019) showed 15% of EGFP-positive cells in rRV-infected MA-NSP5-Csy4 at 12 hpi. EGFP was detected only in cells sustaining viral replication (anti-NSP2) (Figure 4C) and was compromised upon inhibition of viroplasm formation by the proteasome inhibitor MG132 (Contin et al., 2011; Figures 4E and 4F; Figure S6E). EGFP-positive cells were absent in control-infected MA-NSP5-Csy4-H29A (Figure S6F). Following the kinetics of NSP1-EGFP by live-cell imaging, NSP1-EGFP was detected from 6 hpi and increased, reaching a plateau in the number of florescent cells from 13 hpi (Figures 4D and 4F; Video S1). Similar results were obtained scoring the total number of green spots or average number of NSP1-EGFP spots per fluorescent cell (Figure 4E; Figure S6D). Taken together, our data highlight the importance of secondary transcription in RV replication.

DISCUSSION

CRISPR nucleases have been exploited to edit several viral DNA genomes or their DNA replication intermediates, including those of hepatitis B virus, herpesviruses, human papilloma virus, HIV-1, and retroviruses (de Buhr and Lebbink, 2018; Chen et al., 2018; van Diemen et al., 2016; Schiwon et al., 2018; Wang et al., 2016a, 2016b; Yoshiba et al., 2019).

Although RNA targeting nucleases, such as CRISPR-Cas13 and CRISPR-Csy4, and *Francisella novicida* Cas9 have been used to disrupt viral ssRNAs of lymphocytic choriomeningitis virus, influenza A virus, vesicular stomatitis virus, hepatitis C virus, HIV-1, and, lately, SARS-CoV-2 (Abbott et al., 2020; Freije et al., 2019; Guo et al., 2015; Price et al., 2015), there are no reports showing the use of CRISPR nucleases or other homing nucleases for targeting and editing viruses with a dsRNA genome. Among them, the peculiar replication mechanism of RV in hardly accessible viral factories poses several challenges for the effective deployment of nucleic acid editing tools (Silvestri et al., 2004). In addition, there are no known repair mechanisms for a cleaved RV genome nor sequence-specific programmable CRISPR nucleases targeted to dsRNA published yet.

We paved the way for successful nuclease-mediated genome editing of dsRNA viruses by targeting the small and highly specific *P. aeruginosa* CRISPR-Csy4 to cleave the (+)ssRNA intermediates formed within viroplasms, during RV dsRNA genome replication (Borodavka et al., 2017; Patton et al., 2006). This was obtained by fusing Csy4 to the viroplasm-localizing viral proteins NSP5 and NSP2 (Eichwald et al., 2004, 2012; Fabbretti et al., 1999). Three of the 11 RV gss (gs5, gs7, and gs10) were engineered to contain the Csy4 target sequence in different locations. Csy4 activity produced discrete deletions in the RV genome, ranging from 21 to 45 nt with efficiency up to 95% in a single round of infection, increasing to 100% in subsequent rounds. Csy4 was very effective also for multiplex editing of at least three different RV gss (gs5, gs7, and gs10), offering the opportunity to simultaneously induce *in vivo* editing isoforms in different viral genes. Editing was observed exclusively on genome segments carrying the target sequence, indicating that Csy4 fusions with NSP5 or NSP2 had no obvious off-target activity to the WT RV genome.

The presence of editing only with viroplasm-localized Csy4 suggests that it occurs within viroplasms and involves the RNA

(B) Electrophoretic pattern of rRV-gs5*-HA genome replicated in the indicated cells at 16 hpi. Red arrow and asterisk indicate, respectively, non-edited and edited gs5*-HA.
(C) Quantification of gs5*-HA editing; means ± SEM (n = 3).
(D) Frequency of Δ21 and Δ36 deletions (36 clones) from MA-NSP5-Csy4 cells at 9 hpi.
(E) Transcript-specific RT-PCR of gs5*-HA (213 bp) and gs5*-HA-Δ36 (177 bp) from MA-NSP5-Csy4 cells at the indicated hpi. The % Δ36 transcripts are means of n = 3 experiments.
(F) Western blot time course of NSP1-SV5-HA (detected with anti-HA) and VP2 from the indicated cells infected with rRV-gs5*-HA. β-actin was used as control.
(G) Is as in (F) using anti-SV5. Red and black asterisks indicate HA-tagged and non-tagged NSP1-SV5, respectively.
(H) Relative expression of the two NSP1 isoforms as in (G); means ± SEM (n = 3).

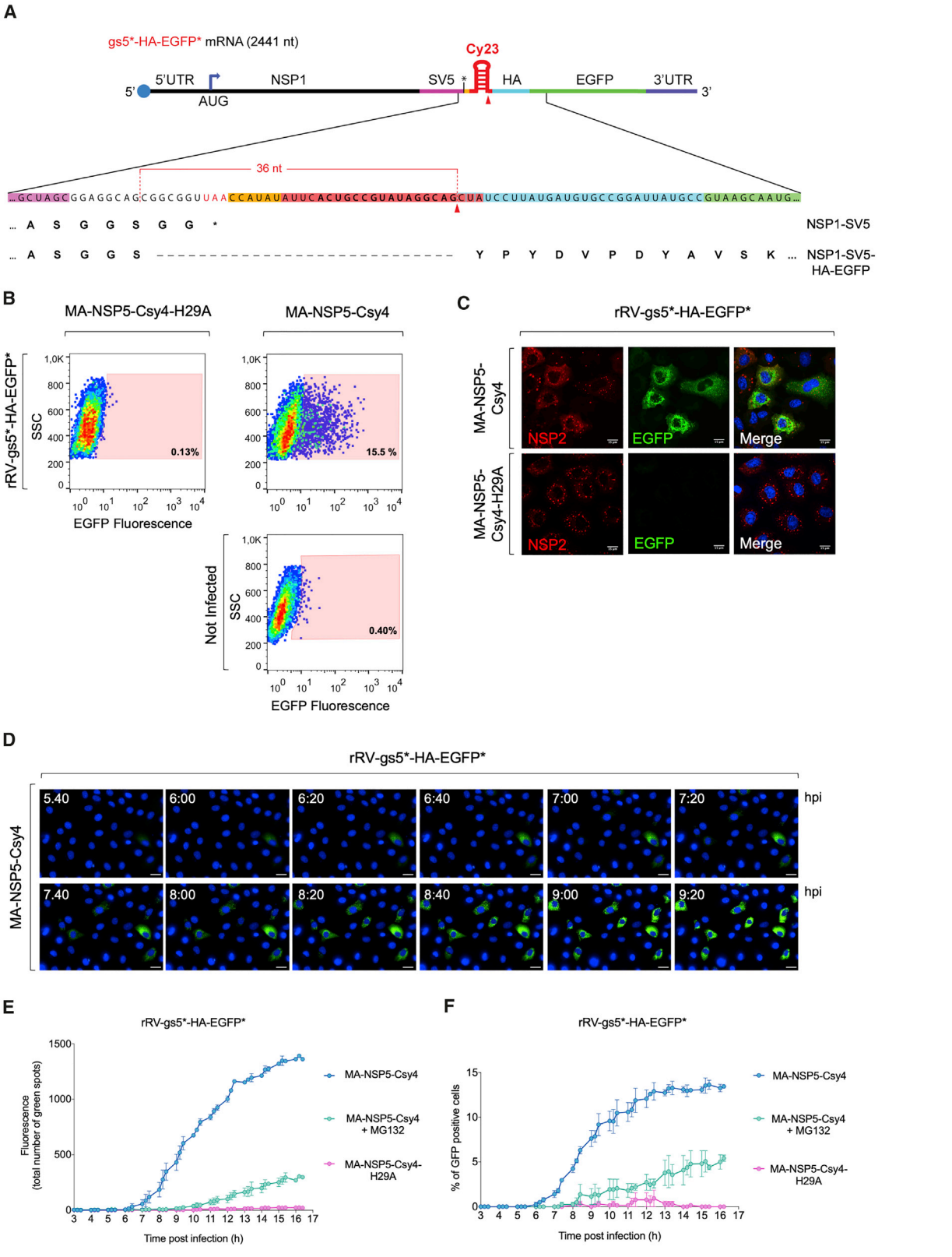

(legend on next page)

replication step. Consistently, RNA interference against RV (+)ssRNAs has never been reported to cause deletions within the target genome segments, probably because viroplasm-localized (+)ssRNAs intermediates are not accessible to the RNA-induced silencing complex (RISC) complex (Campagna et al., 2005; Silvestri et al., 2004).

In all the editing events, the sequence downstream of the Csy4 cleavage site, including the 3′ UTR, was preserved, suggesting a repair mechanism for the Csy4-cleaved (+)ssRNA replication intermediate. The edited sequences contained a deletion for which the 3′ end corresponded exactly to the Csy4 cleavage site, after the G positioned at the base of the stem structure on the targeted RNA.

At the 5′ end, all deletions started after a G nucleotide (Figure S7A), which seems to be important for the generation of the edited genome segment, as removing a specific G involved in a precise deletion completely prevented that editing outcome and, in some cases, enabled new deletions involving other proximal G residues.

We envisaged two possible alternative mechanisms for the generation of the deleted dsRNA: (1) the Csy4-cleaved (+)ssRNA undergoes a second upstream cleavage by an unidentified nuclease that is followed by a cytosolic splicing ligation of the two newly generated 5′ and 3′ fragments (Figure S7B, top panel). The repaired (+)ssRNA would then serve as template to generate the edited dsRNA; (2) alternatively, the deletion takes place during synthesis of the minus strand by the RNA-dependent RNA polymerase (RdRp) VP1 within replication complexes. Also in this case, the Csy4-mediated cleavage might be followed by a second upstream cleavage on the (+)ssRNA strand (without the need of a ligation) and by VP1 synthesis of the complete negative strand harboring the deletion. The latter would then serve to produce deleted (+)ssRNA in a secondary-transcription-dependent manner (Figure S7B, top panel). It is very unlikely that the putative second cleavages could represent Csy4 off-target sites, as Csy4 has a very strict substrate recognition sequence (Haurwitz et al., 2010; Sternberg et al., 2012; Lee et al., 2013).

We applied the *in vivo* editing of the dsRNA RV genome to address an important question related to the RV replication cycle: the contribution of transcription by the newly made viral DLPs during infection (Desselberger, 2014; Estes and Greenberg, 2013; López et al., 2005), which cannot be addressed only by reverse genetics. In the case of RV and of members of the *Orthoreovirus* genus, secondary transcription is not easily addressed, as the progeny virus has exactly the same genetic composition as the infecting particles (Acs et al., 1971; Sakuma and Watanabe, 1971).

By building rRV containing either gs5* encoding an NSP1-HA, or an EGFP reporter, which could be expressed only following Csy4-mediated editing, we monitored secondary transcription by proteomic and live-cell imaging approaches. Secondary transcription was detected from 5 hpi, and the translation products of secondary transcripts were clearly visible from 6–7 hpi. At 9 hpi, we found that the contribution of secondary transcription and translation was responsible for a large fraction of the newly made gs5-derived transcripts (63%) and proteins (70%), suggesting that the efficiency of virus replication is governed by the capacity of the newly assembled DLPs to produce translation competent viral mRNAs. Impairment of viral replication by MG132 treatment strongly compromised the detection of secondary transcription products, supporting the idea that Csy4-mediated RV editing requires active viral replication.

The recent development of different reverse genetics protocols for RV represents a powerful tool to investigate virus biology (Kanai et al., 2017; Komoto et al., 2018; Papa et al., 2019). The nuclease-mediated editing of dsRNA virus could overcome current limitations of reverse genetics systems or be combined with them for new applications, for example producing many edited virus variants unachievable directly by reverse genetics.

Overall, our data represent the description of nuclease-mediated editing of a dsRNA viral genome. The *in vivo* generation of recombinant RVs with edited genomes paves the way for harnessing this tool to study different aspects of viral replication, as well as its use for the identification of therapeutic drugs targeting the assembly of DLPs or other pathways associated with secondary transcription.

STAR★METHODS

Detailed methods are provided in the online version of this paper and include the following:

- KEY RESOURCES TABLE
- RESOURCE AVAILABILITY
  - Lead Contact
  - Materials Availability
  - Data and Code Availability
- EXPERIMENTAL MODEL AND SUBJECT DETAILS
  - Cell lines
  - Plasmids
- METHOD DETAILS
  - Generation of stable cell lines
  - Rescue of recombinant RVs from cloned cDNAs
  - Replication kinetics of recombinant viruses
  - EGFP-plasmid based transcript cleavage assay
  - Western blot
  - Immunofluorescence

Figure 4. Csy4-Mediated Live-Cell Imaging of RV Secondary Transcription and Translation

(A) Scheme of the gs5*-HA-EGFP* (+)ssRNA showing the Δ36 deletion required for EGFP expression.

(B) The % of EGFP-positive cells non-infected or infected with rRV-gs5*-HA-EGFP* (MOI, 5) determined by cytofluorimetry at 12 hpi.

(C) Immunofluorescence of cells infected as in (B). Infected cells and viroplasms were detected with anti-NSP2 (red). Scale bar, 13 μm.

(D) Time course of EGFP fluorescence (from 5:40 to 9:20 hpi) of rRV-gs5*-HA-EGFP infected MA-NSP5-Csy4 cells. Scale bar, 20 μm. In (C) and (D), nuclei stained with 4',6-diamidin-2-fenilindolo (DAPI) (blue).

(E) Live-cell imaging quantification of the total number of NSP1-EGFP spots in MA-NSP5-Csy4 cells (+/− MG132) and MA-NSP5-Csy4-H29A cells infected with rRV-gs5-HA-EGFP* (MOI, 5).

(F) Percentage of EGFP fluorescent cells (all cells scoring a number of NSP1-EGFP positive spots of ≥ 1) as in (E).

- Electrophoresis of viral dsRNA genomes
- dsRNA extraction from polyacrylamide gels
- Cytofluorimetry
- Live Cells imaging
- Sequencing of edited RV genomic segments
- PCR using splicing primers

- QUANTIFICATION AND STATISTICAL ANALYSIS
  - Statistical Analysis

SUPPLEMENTAL INFORMATION

Supplemental Information can be found online at https://doi.org/10.1016/j.celrep.2020.108205.

ACKNOWLEDGMENTS

The authors are grateful to Shan Tang and Josè Luis Slon Campos for critical reading of this manuscript and Naoto Ito for providing BHK-T7 cells. This work was supported by ICGEB intramural funding. G. Papa and E.S. were supported by a ICGEB pre-doctoral fellowship. Some figures were created with BioRender.com.

AUTHOR CONTRIBUTIONS

Experiments were mainly conducted by G. Papa with the help of L.V. Live-cell imaging analysis was carried out by G. Papa, L.B., E.S., and M.G. O.R.B., G. Papa, and G. Petris planned the project and wrote the manuscript. All authors read, corrected, and approved the final manuscript.

DECLARATION OF INTERESTS

The authors declare no competing interests.

Received: March 11, 2020
Revised: June 14, 2020
Accepted: September 4, 2020
Published: September 29, 2020

REFERENCES

Abbott, T.R., Dhamdhere, G., Liu, Y., Lin, X., Goudy, L., Zeng, L., Chemparathy, A., Chmura, S., Heaton, N.S., Debs, R., et al. (2020). Development of CRISPR as an Antiviral Strategy to Combat SARS-CoV-2 and Influenza. Cell *181*, 865–876.e12.

Acs, G., Klett, H., Schonberg, M., Christman, J., Levin, D.H., and Silverstein, S.C. (1971). Mechanism of reovirus double-stranded ribonucleic acid synthesis in vivo and in vitro. J. Virol. *8*, 684–689.

Barro, M., and Patton, J.T. (2007). Rotavirus NSP1 inhibits expression of type I interferon by antagonizing the function of interferon regulatory factors IRF3, IRF5, and IRF7. J. Virol. *81*, 4473–4481.

Borchardt, E.K., Vandoros, L.A., Huang, M., Lackey, P.E., Marzluff, W.F., and Asokan, A. (2015). Controlling mRNA stability and translation with the CRISPR endoribonuclease Csy4. RNA *21*, 1921–1930.

Borodavka, A., Dykeman, E.C., Schrimpf, W., and Lamb, D.C. (2017). Protein-mediated RNA folding governs sequence-specific interactions between rotavirus genome segments. eLife *6*, 1–22.

Brinkman, E.K., Chen, T., Amendola, M., and van Steensel, B. (2014). Easy quantitative assessment of genome editing by sequence trace decomposition. Nucleic Acids Res. *42*, e168.

Campagna, M., Eichwald, C., Vascotto, F., and Burrone, O.R. (2005). RNA interference of rotavirus segment 11 mRNA reveals the essential role of NSP5 in the virus replicative cycle. J. Gen. Virol. *86*, 1481–1487.

Chen, Y.C., Sheng, J., Trang, P., and Liu, F. (2018). Potential application of the CRISPR/CAS9 system against herpesvirus infections. Viruses *10*, 291.

Contin, R., Arnoldi, F., Campagna, M., and Burrone, O.R. (2010). Rotavirus NSP5 orchestrates recruitment of viroplasmic proteins. J. Gen. Virol. *91*, 1782–1793.

Contin, R., Arnoldi, F., Mano, M., and Burrone, O.R. (2011). Rotavirus Replication Requires a Functional Proteasome for Effective Assembly of Viroplasms. *85*, 2781–2792.

Davis, K.A., and Patton, J.T. (2017). Shutdown of interferon signaling by a viral-hijacked E3 ubiquitin ligase. Microb. Cell *4*, 387–389.

de Buhr, H., and Lebbink, R.J. (2018). Harnessing CRISPR to combat human viral infections. Curr. Opin. Immunol. *54*, 123–129.

Desselberger, U. (1996). Genome rearrangements of rotaviruses. Arch. Virol. Suppl. *12*, 37–51.

Desselberger, U. (2014). Rotaviruses. Virus Res. *190*, 75–96.

Eichwald, C., Rodriguez, J.F., and Burrone, O.R. (2004). Characterization of rotavirus NSP2/NSP5 interactions and the dynamics of viroplasm formation. J. Gen. Virol. *85*, 625–634.

Eichwald, C., Arnoldi, F., Laimbacher, A.S., Schraner, E.M., Fraefel, C., Wild, P., Burrone, O.R., and Ackermann, M. (2012). Rotavirus viroplasm fusion and perinuclear localization are dynamic processes requiring stabilized microtubules. PLoS One *7*, e47947.

Estes, M.K., and Greenberg, H.B. (2013). Rotaviruses. In Fields Virology, David M. Knipe and Peter M. Howley, eds. (Philadelphia: W.K. Health and Lippincott Williams & Wilkins), pp. 1347–1401.

Fabbretti, E., Afrikanova, I., Vascotto, F., and Burrone, O.R. (1999). Two non-structural rotavirus proteins, NSP2 and NSP5, form viroplasm-like structures in vivo. J. Gen. Virol. *80*, 333–339.

Freije, C.A., Myhrvold, C., Boehm, C.K., Lin, A.E., Welch, N.L., Carter, A., Metsky, H.C., Luo, C.Y., Abudayyeh, O.O., Gootenberg, J.S., et al. (2019). Programmable Inhibition and Detection of RNA Viruses Using Cas13. Mol. Cell *76*, 826–837.e11.

Giambiagi, S., González Rodríguez, I., Gómez, J., and Burrone, O. (1994). A rearranged genomic segment 11 is common to different human rotaviruses. Arch. Virol. *136*, 415–421.

González, S.A., Mattion, N.M., Bellinzoni, R., and Burrone, O.R. (1989). Structure of rearranged genome segment 11 in two different rotavirus strains generated by a similar mechanism. J. Gen. Virol. *70*, 1329–1336.

Gray, J., and Desselberger, U. (2000). Rotaviruses (Humana Press).

Guo, R., Wang, H., Cui, J., Wang, G., Li, W., and Hu, J.F. (2015). Inhibition of HIV-1 Viral Infection by an Engineered CRISPR Csy4 RNA Endoribonuclease. PLoS One *10*, e0141335.

Haurwitz, R.E., Jinek, M., Wiedenheft, B., Zhou, K., and Doudna, J.A. (2010). Sequence- and structure-specific RNA processing by a CRISPR endonuclease. Science *329*, 1355–1358.

Haurwitz, R.E., Sternberg, S.H., and Doudna, J.A. (2012). Csy4 relies on an unusual catalytic dyad to position and cleave CRISPR RNA. EMBO J. *31*, 2824–2832.

Jinek, M., Chylinski, K., Fonfara, I., Hauer, M., Doudna, J.A., and Charpentier, E. (2012). A programmable dual-RNA-guided DNA endonuclease in adaptive bacterial immunity. Science *337*, 816–821.

Kanai, Y., Komoto, S., Kawagishi, T., Nouda, R., Nagasawa, N., Onishi, M., Matsuura, Y., Taniguchi, K., and Kobayashi, T. (2017). Entirely plasmid-based reverse genetics system for rotaviruses. Proc. Natl. Acad. Sci. USA *114*, 2349–2354.

Komoto, S., Fukuda, S., Ide, T., Ito, N., Sugiyama, M., Yoshikawa, T., Murata, T., and Taniguchi, K. (2018). Generation of Recombinant Rotaviruses Expressing Fluorescent Proteins by Using an Optimized Reverse Genetics System. J. Virol. *92*, e00588-18.

Lee, H.Y., Haurwitz, R.E., Apffel, A., Zhou, K., Smart, B., Wenger, C.D., Laderman, S., Bruhn, L., and Doudna, J.A. (2013). RNA-protein analysis using a conditional CRISPR nuclease. Proc. Natl. Acad. Sci. USA *110*, 5416–5421.

López, T., Camacho, M., Zayas, M., Nájera, R., Sánchez, R., Arias, C.F., and López, S. (2005). Silencing the morphogenesis of rotavirus. J. Virol. *79*, 184–192.

Makarova, K.S., Wolf, Y.I., and Koonin, E.V. (2018). Classification and Nomenclature of CRISPR-Cas Systems: Where from Here? CRISPR J. *1*, 325–336.

Méndez, E., Arias, C.F., and López, S. (1992). Genomic rearrangements in human rotavirus strain Wa; analysis of rearranged RNA segment 7. Arch. Virol. *125*, 331–338.

Murphy, S.K., and Arnold, M.M. (2019). Rotavirus NSP1 localizes in the nucleus to disrupt PML nuclear bodies during infection. bioRxiv. https://doi.org/10.1101/619932.

Murugan, K., Babu, K., Sundaresan, R., Rajan, R., and Sashital, D.G. (2017). The Revolution Continues: Newly Discovered Systems Expand the CRISPR-Cas Toolkit. Mol. Cell *68*, 15–25.

Nissim, L., Perli, S.D., Fridkin, A., Perez-Pinera, P., and Lu, T.K. (2014). Multiplexed and programmable regulation of gene networks with an integrated RNA and CRISPR/Cas toolkit in human cells. Mol. Cell *54*, 698–710.

Özcan, A., Pausch, P., Linden, A., Wulf, A., Schühle, K., Heider, J., Urlaub, H., Heimerl, T., Bange, G., and Randau, L. (2019). Type IV CRISPR RNA processing and effector complex formation in Aromatoleum aromaticum. Nat. Microbiol. *4*, 89–96.

Papa, G., Venditti, L., Arnoldi, F., Schraner, E.M., Potgieter, C., Borodavka, A., Eichwald, C., and Burrone, O.R. (2019). Recombinant rotaviruses rescued by reverse genetics reveal the role of NSP5 hyperphosphorylation in the assembly of viral factories. J. Virol. *94*, e01110–e01119.

Patton, J.T., Silvestri, L.S., Tortorici, M.A., Vasquez-Del Carpio, R., and Taraporewala, Z.F. (2006). Rotavirus genome replication and morphogenesis: role of the viroplasm. Curr. Top. Microbiol. Immunol. *309*, 169–187.

Petris, G., Bestagno, M., Arnoldi, F., and Burrone, O.R. (2014). New tags for recombinant protein detection and O-glycosylation reporters. PLoS One *9*, e96700.

Price, A.A., Sampson, T.R., Ratner, H.K., Grakoui, A., and Weiss, D.S. (2015). Cas9-mediated targeting of viral RNA in eukaryotic cells. Proc. Natl. Acad. Sci. USA *112*, 6164–6169.

Sakuma, S., and Watanabe, Y. (1971). Unilateral synthesis of reovirus double-stranded ribonucleic acid by a cell-free replicase system. J. Virol. *8*, 190–196.

Schiwon, M., Ehrke-Schulz, E., Oswald, A., Bergmann, T., Michler, T., Protzer, U., and Ehrhardt, A. (2018). One-Vector System for Multiplexed CRISPR/Cas9 against Hepatitis B Virus cccDNA Utilizing High-Capacity Adenoviral Vectors. Mol. Ther. Nucleic Acids *12*, 242–253.

Schnepf, N., Deback, C., Dehee, A., Gault, E., Parez, N., and Garbarg-Chenon, A. (2008). Rearrangements of rotavirus genomic segment 11 are generated during acute infection of immunocompetent children and do not occur at random. J. Virol. *82*, 3689–3696.

Silvestri, L.S., Taraporewala, Z.F., and Patton, J.T. (2004). Rotavirus replication: plus-sense templates for double-stranded RNA synthesis are made in viroplasms. J. Virol. *78*, 7763–7774.

Sternberg, S.H., Haurwitz, R.E., and Doudna, J.A. (2012). Mechanism of substrate selection by a highly specific CRISPR endoribonuclease. RNA *18*, 661–672.

Troupin, C., Schnuriger, A., Duponchel, S., Deback, C., Schnepf, N., Dehee, A., and Garbarg-Chenon, A. (2011). Rotavirus rearranged genomic RNA segments are preferentially packaged into viruses despite not conferring selective growth advantage to viruses. PLoS One *6*, e20080.

van Diemen, F.R., Kruse, E.M., Hooykaas, M.J.G., Bruggeling, C.E., Schürch, A.C., van Ham, P.M., Imhof, S.M., Nijhuis, M., Wiertz, E.J.H.J., and Lebbink, R.J. (2016). CRISPR/Cas9-Mediated Genome Editing of Herpesviruses Limits Productive and Latent Infections. PLoS Pathog. *12*, e1005701.

Wang, G., Zhao, N., Berkhout, B., and Das, A.T. (2016a). A Combinatorial CRISPR-Cas9 Attack on HIV-1 DNA Extinguishes All Infectious Provirus in Infected T Cell Cultures. Cell Rep. *17*, 2819–2826.

Wang, Z., Pan, Q., Gendron, P., Zhu, W., Guo, F., Cen, S., Wainberg, M.A., and Liang, C. (2016b). CRISPR/Cas9-Derived Mutations Both Inhibit HIV-1 Replication and Accelerate Viral Escape. Cell Rep. *15*, 481–489.

Wu, W., Orr-Burks, N., Karpilow, J., and Tripp, R.A. (2017). Development of improved vaccine cell lines against rotavirus. Sci. Data *4*, 170021.

Yoshiba, T., Saga, Y., Urabe, M., Uchibori, R., Matsubara, S., Fujiwara, H., and Mizukami, H. (2019). CRISPR/Cas9-mediated cervical cancer treatment targeting human papillomavirus E6. Oncol. Lett. *17*, 2197–2206.

Yusa, K., Zhou, L., Li, M.A., Bradley, A., and Craig, N.L. (2011). A hyperactive piggyBac transposase for mammalian applications. Proc. Natl. Acad. Sci. USA *108*, 1531–1536.

STAR★METHODS

KEY RESOURCES TABLE

REAGENT or RESOURCE	SOURCE	IDENTIFIER
Antibodies		
anti-SV5 mAb	Life Technologies	Cat# R960-25; RRID:AB_2556564
anti-HA mAb clone HA-7	Sigma-Aldrich	Cat# H3663; RRID:AB_262051
anti-NSP5 guinea pig serum	Contin et al., 2010	N/A
anti-NSP5 roTag mAb	Petris et al., 2014	N/A
anti-VP2 guinea pig serum	Eichwald et al., 2004	N/A
HRP-conjugated goat anti-guinea pig	Jackson ImmunoResearch	Cat# 106-035-003; RRID:AB_2337402
HRP-goat anti-mouse IgG	KPL	Cat# 5220-0341
HRP-conjugated anti-GAPDH mAb clone sc-47724	Santa Cruz Biotechnology	Cat# sc-47724; RRID:AB_627678
Mouse HRP-conjugated anti-actin mAb clone AC-15	Sigma-Aldrich	Cat# A1978; RRID:AB_476692
Bacterial and Virus Strains		
rRV-wt	This paper	N/A
rRV-gs5*	This paper	N/A
rRV-gs7*	This paper	N/A
rRV-gs10*	This paper	N/A
rRV-gs5*-HA	This paper	N/A
rRV-gs5*/284	This paper	N/A
rRV-gs5*-HA-EGFP*	This paper	N/A
rRV-gs5*-GA	This paper	N/A
E.coli DH5α	Thermo Fisher Scientific	Cat# 18265017
Chemicals, Peptides, and Recombinant Proteins		
RNAzol	Sigma-Aldrich	Cat# R4533
Experimental Models: Cell Lines		
MA104	ATCC	Cat# CRL-2378.1
MA-NSP5-Csy4	This paper	N/A
MA-NSP5-Csy4-H29A	This paper	N/A
MA-Csy4	This paper	N/A
MA-Csy4-H29A	This paper	N/A
MA-NSP2-Csy4	This paper	N/A
MA-NSP2-mCherry	Papa et. al, 2019	N/A
BHK-T7	Naoto Ito	N/A
Oligonucleotides		
Primers for plasmid construction, see Table S1	This paper	N/A
Recombinant DNA		
pT7-VP1-SA11	Kanai et al., 2017	N/A
pT7-VP2-SA11	Kanai et al., 2017	N/A
pT7-VP3-SA11	Kanai et al., 2017	N/A
pT7-VP4-SA11	Kanai et al., 2017	N/A
pT7-VP7-SA11	Kanai et al., 2017	N/A
pT7-NSP1-SA11	Kanai et al., 2017	N/A
pT7-NSP2-SA11	Kanai et al., 2017	N/A
pT7-NSP3-SA11	Kanai et al., 2017	N/A
pT7-NSP4-SA11	Kanai et al., 2017	N/A
pT7-NSP5-SA11	Kanai et al., 2017	N/A

(*Continued on next page*)

Continued

REAGENT or RESOURCE	SOURCE	IDENTIFIER
pT7-gs5*	This paper	N/A
pT7-gs5*-GA	This paper	N/A
pT7-gs7*	This paper	N/A
pT7-gs10*	This paper	N/A
pT7-gs5*/284	This paper	N/A
pT7-gs5*-HA	This paper	N/A
pT7-gs5*-HA-EGFP*	This paper	N/A
pPB-MCS	Papa et. al, 2019	N/A
pPB-NSP5-SV5-Csy4	This paper	N/A
pPB-SV5-Csy4	This paper	N/A
pPB-NSP5-SV5-Csy4-H29A	This paper	N/A
pPB-SV5-Csy4-H29A	This paper	N/A
pPB-NSP2-SV5-Csy4	This paper	N/A
Software and Algorithms		
FlowJo Software	Becton, Dickinson and Company 2019	RRID:SCR_008520
GraphPad Prism 7 GraphPad	GraphPad	RRID:SCR_002798
TIDE software	Brinkman et al., 2014	N/A
Image Lab Software 6.0.1	Bio-Rad	RRID:SCR_014210
Columbus analysis software	Perkinelmer	N/A

RESOURCE AVAILABILITY

Lead Contact

Further information and requests for resources and reagents, which may require a completed Materials Transfer Agreement, should be directed to and will be fulfilled by the Lead Contact, Oscar R. Burrone (burrone@icgeb.org).

Materials Availability

Processed data associated with this study are present in the paper. Other new material associated with this study are available from the lead author upon request.

Data and Code Availability

This study did not generate any unique datasets or code.

EXPERIMENTAL MODEL AND SUBJECT DETAILS

Cell lines

MA104 (embryonic African green monkey kidney cells ATCC CRL-2378.1) cells were cultured in Dulbecco's Modified Eagle's Medium (DMEM) (Life Technologies) supplemented with 10% Fetal Bovine Serum (FBS) (Life Technologies) and 50 μg/ml gentamycin (Biochrom AG).

MA104-NSP5-Csy4 (MA-NSP5-Csy4), MA104-NSP5-Csy4-H29A (MA-NSP5-Csy4-H29A), MA104-Csy4 (MA-Csy4), MA104-Csy4-H29A (MA-Csy4-H29A), MA104-NSP2-Csy4 (MA-NSP2-Csy4), MA104-NSP2-mCherry (MA-NSP2-mCherry) stable transfectant cell lines were grown in DMEM containing 10% FBS, 50 μg/ml gentamycin and 5 μg/ml puromycin (Sigma-Aldrich).

BHK-T7 cells (Baby Hamster Kidney stably expressing T7 RNA polymerase) were cultured in Glasgow medium supplemented with 5% FBS, 10% Tryptose Phosphate Broth (TPB) (Sigma-Aldrich), 50 μg/ml gentamycin, 2% Non-Essential Amino Acids (NEAA) and 1% Glutamine.

Plasmids

RV plasmids pT7-VP1-SA11, pT7-VP2-SA11, pT7-VP3-SA11, pT7-VP4-SA11, pT7-VP6-SA11, pT7-VP7-SA11, pT7-NSP1-SA11, pT7-NSP2-SA11, pT7-NSP3-SA11, pT7-NSP4-SA11, and pT7-NSP5-SA11 (Kanai et al., 2017; Komoto et al., 2018) were used to rescue recombinant RVs by reverse genetics.

pPB-NSP5-SV5-Csy4 and pPB-SV5-Csy4 plasmids were obtained from a GenParts DNA fragment (Genscript) containing NSP5-SV5-Csy4 and SV5-Csy4 and inserted in the pPB-MCS vector (Papa et al., 2019) using BamHI-XmaI restriction enzymes sites.

pPB-NSP5-SV5-Csy4-H29A and pPB-SV5-Csy4-H29A plasmids carrying two nucleotides substitutions C82G and A83C in the Csy4 ORF were generated by QuikChange II Site-Directed Mutagenesis (Agilent Technologies) from the pPB-NSP5-SV5-Csy4 and pPB-SV5-Csy4 respectively using Csy4-H29A-FOR and Csy4-H29A-REV primers (Table S1).

A GenParts DNA fragment containing the NSP2-SV5-Csy4 was inserted into pPB-MCS vector using NotI-EcoRI restriction enzymes sites to obtain the pPB-NSP2-SV5-Csy4.

pEGFP-Cy28 was generated inserting Cy28 after the ATG into the pEGFP-C1 plasmid (Addgene) using the pEGFP-Cy28-FOR and pEGFP-Cy28-REV primers (Table S1) for QuikChange II Site-Directed Mutagenesis.

pT7-gs5* was generated inserting a GenParts DNA fragment into the pT7-NSP1-SA11 using PacI-BamHI restriction enzymes sites. This GenParts fragment contains the SV5 tag and Cy28 at position 1518 of the gs5. pT7-gs5*-GA was synthetized as above with a point mutation of G into an A at position 1580.

pT7-gs7* was generated inserting a GenParts DNA fragment into the pT7-NSP3-SA11 using SnaBI-SacI restriction enzymes sites. The GenParts fragment contains the SV5 tag and Cy28 at position 970 of the gs7.

pT7-gs10* was generated from pT7-NSP4-SA11 inserting Cy28 sequence using gs10*-Cy28-FOR and gs10*-Cy28-REV primers by QuikChange II Site-Directed Mutagenesis.

For the generation of pT7-gs5*/284, a GenParts DNA fragment containing the SV5 tag and Cy28 was inserted into pT7-NSP1-SA11 using MfeI-BamHI restriction enzymes sites. pT7-gs5*-HA was obtained inserting a GenParts DNA fragment including the SV5 tag, Cy23 and the HA tag in plasmid pT7-NSP1-SA11 using MfeI-BamHI restriction enzymes sites. pT7-gs5*-HA-EGFP* was generated cloning a GenParts DNA fragment into the pT7-NSP1-SA11 using MfeI-BamHI. The GenParts contains the SV5 tag, Cy23, the HA tag and the EGFP ORF upstream of the 3′UTR of gs5.

METHOD DETAILS

Generation of stable cell lines

MA-NSP2-mCherry cells were previously described (Papa et al., 2019). MA-NSP5-Csy4, MA-NSP5-Csy4-H29A, MA-Csy4, MA-Csy4-H29A, MA-NSP2-Csy4 were similarly generated by PiggyBac Technology (Papa et al., 2019; Yusa et al., 2011). Briefly, MA104 cells (10^5) were seeded in a 12 Multi-well plate, transfected the next day with the pCMV-HyPBase (0.5 μg) and the respective transposon plasmids: pPB-NSP5-SV5-Csy4, pPB-NSP5-SV5-Csy4-H29A, pPB-SV5-Csy4, pPB-SV5-Csy4-H29A and pPB-NSP2-SV5-Csy4, using a ratio of 1:2.5 respectively with Lipofectamine 3000 (Sigma-Aldrich) according to the manufacturer's instructions.

Cells were maintained in DMEM supplemented with 10% FBS for 3 days and then incubated with DMEM supplemented with 10% FBS and 10 μg/ml puromycin for 4 days for selection.

Rescue of recombinant RVs from cloned cDNAs

To rescue recombinant RV strain SA11 (rRV-wt), monolayers of BHK-T7 cells (4×10^5) cultured in 12-well plates were co-transfected using 2.5 μL of TransIT-LT1 transfection reagent (Mirus) per microgram of DNA plasmid. Each mixture comprised 0.8 μg of SA11 rescue plasmids: pT7-VP1, pT7-VP2, pT7-VP3, pT7- VP4, pT7-VP6, pT7-VP7, pT7-NSP1, pT7-NSP3, pT7-NSP4, and 2.4 μg of pT7-NSP2 and pT7-NSP5 (Kanai et al., 2017; Komoto et al., 2018). Furthermore 0.8 μg of pcDNA3-NSP2 and 0.8 μg of pcDNA3-NSP5, encoding NSP2 and NSP5 proteins, were also co-transfected to increase rescue efficiency (Papa et al., 2019). To rescue recombinant rRVs having modified genomic segments, pT7-gs5*, pT7-gs5*-GA, pT7-gs5*/284, pT7-gs5*-HA, pT7-gs5*-HA-EGFP*, pT7-gs7*, pT7-gs10* plasmids were used instead of pT7-NSP1-SA11, pT7-NSP3-SA11, pT7-NSP4-SA11 respectively.

Cells were co-cultured with MA104 cells for 3 days in FBS-free medium supplemented with trypsin from porcine pancreas (0.5 μg/ml final concentration) (T0303-Sigma Aldrich) and lysed by freeze-thawing. 300 μL of the lysate was transferred to fresh MA104 wt cells, further cultured at 37°C for 4 days in FBS-free DMEM supplemented with 0.5 μg/ml trypsin until a clear cytopathic effect was visible. The modified genome segments of rescued recombinant rotaviruses were sequenced.

Replication kinetics of recombinant viruses

MA104 cells were seeded into 24-well plates, infected with rRVs at MOI of 0.5 for multi-step growth curve experiments. Cells were harvested after 6, 12, 24, 36 hours post infection and lysed by freeze-thawing three times and activated with trypsin (1 μg/ml) for 30 min at 37°C. The lysates were used to infect monolayers of MA104 stably expressing the fusion protein NSP2-mCherry (Papa et al., 2019). The MA-NSP2-mCherry cells were seeded in μ-Slide 8 Well Chamber Slide-well (iBidi GmbH) and infected with dilutions of virus-containing lysates. Cells were then fixed 5 hours after the infection for 15 min with 4% paraformaldehyde. Nuclei were then stained with ProLong Diamond Antifade Mountant with DAPI (Thermo Scientific). Samples were imaged using a confocal setup (Zeiss Airyscan equipped with a 63x, NA = 1.3 objective). Each viroplasms-containing cell was counted as one focus-forming unit (FFU). The average of cells with viroplasms of six fields of view per each virus dilution was determined and the total number of cells containing viroplasms in the whole preparation was estimated. The virus titer was determined as previously described (Eichwald et al., 2012).

EGFP-plasmid based transcript cleavage assay

MA104, MA-NSP5-Csy4, MA-NSP5-Csy4-H29A, MA-NSP2-Csy4, MA-Csy4, MA-Csy4-H29A were seeded at a density of $2x10^5$ in a 12 Multi-well plate and transfected with 0.5 μg of pEGFP-Cy28 or pEGFP plasmid using Lipofectamine 3000 following manufactures'

instructions. The cells were imaged 24 hours post-transfection using a Nikon Eclipse (Ti-E, Nikon, Japan). The images were acquired and GFP expression was analyzed and quantified using ImageJ software.

Western blot

Samples from rRV-infected cells were run in reducing 10% or 7%–15% gradient SDS-PAGE, transferred to polyvinylidene difluoride (PVDF) membranes (Millipore) and blocked in a 5% milk solution in PBS (PBS-milk) for 30 minutes. SV5-tagged proteins were detected using mouse anti-SV5 mAb (1:5000, Life Technologies); HA-tagged proteins were detected by anti-HA mAb (clone HA-7, 1:5000, Sigma-Aldrich); NSP5 and VP2 proteins were detected using anti-NSP5 guinea pig serum (1:5000) or anti-NSP5 roTag mAb and anti-VP2 guinea pig serum (1:2000) (Contin et al., 2010; Eichwald et al., 2004; Petris et al., 2014). As secondary antibodies were used HRP-conjugated goat anti-guinea pig (1:10000; Jackson ImmunoResearch) or goat anti-mouse IgG antibodies (1:10000; KPL).

Mouse HRP-conjugated anti-GAPDH mAb (clone sc-47724, Santa Cruz Biotechnology, 1:1000) and Mouse HRP-conjugated anti-actin mAb (clone AC-15, Sigma-Aldrich, 1:40000) were used as loading controls. Membranes were developed by Enhanced Chem-iLuminescence System (Pierce ECL-Western blotting system, ThermoFisher-Pierce). Quantification analysis of bands were carried out using ImageLab 6.0.1 (Bio-Rad).

Immunofluorescence

Immunofluorescence experiments were performed using μ-Slide 8 Well Chamber Slide-well (iBidi GmbH). Cells were washed three times with PBS, treated with paraformaldehyde 3.7% in PBS for 15 minutes, cells were then incubated with 0.1% Triton X-100 (Sigma) in PBS for 5 minutes followed by incubation with 1% BSA for 30 minutes. For the detection of proteins, cells were incubated with primary antibody diluted in 1% PBS-BSA for 1 hour, washed three times with PBS and then incubated with secondary antibody for 45 minutes. Nuclei were then stained with ProLong Diamond Antifade Mountant with DAPI (Thermo Scientific) and the slides were imaged using a confocal setup (Zeiss Airyscan equipped with a 63x, NA = 1.3 objective). Antibodies were used at the following dilutions: mouse anti-SV5 mAb (1:1000); anti-NSP5 guinea pig serum 1:1000; anti-NSP2 guinea pig serum 1:200 (Contin et al., 2010; Eichwald et al., 2004); Alexa Fluor 488-conjugated anti-mouse, 1:500 (Life Technologies), and TRITC-conjugated anti-guinea pig, 1:500 (Life Technologies). Quantification analysis were performed using ImageJ software.

Electrophoresis of viral dsRNA genomes

Total RNA was extracted with RnaZol® (Sigma-Aldrich) from cells infected at MOI of 5 and lysed at 16 hours post infection. The RNA was run on a 10% poly-acrylamide denaturing gels (PAGE) for 2 hours at 180 Volts. The gel was than stained with ethidium bromide (1 μg/ml) and the dsRNA pattern was visualized using the ChemiDoc Imaging System (Gray and Desselberger, 2000). Quantification analysis of bands were carried out using ImageLab 6.0.1.

dsRNA extraction from polyacrylamide gels

The bands of interest from a polyacrylamide gel were cut, crushed with a pipette and placed in 1.5 mL tubes. 300 μL of elution buffer (0.5 M NH4OAc, 0.1% SDS, 10 mM Tris-HCl pH 8.0, 1 mM EDTA) was added, mixed for 2 hours and then centrifuged 3 times at 5000 g for 1 minute to pellet the acrylamide residues. The RNA was precipitated with 1 volume of 3M NaOAc pH 5.2 and 3 volumes of 100% EtOH, centrifuged at 16000 g for 30 minutes, washed twice with 2 volumes of 70% EtOH, and resuspended in RNase free water. The dsRNA was denaturated, retro-transcribed, PCR amplified and cloned into a pcDNA 3.1 plasmid (Invitrogen) for sequencing.

Cytofluorimetry

MA-NSP5-Csy4 and MA-NSP5-Csy4-H29A were infected with rRV-gs5*-HA-EGFP* at MOI of 5 and collected 12 hours post infection. Cells were trypsinised, washed twice with PBS, centrifuged for 5 minutes at 200 g and resuspended in PBS. EGFP fluorescence was analyzed using a FACS Calibur cytofluorimeter (BD Biosciences).

Live Cells imaging

MA-NSP5-Csy4 and MA-NSP5-Csy4-H29A cells ($2x10^3$) were seeded into CellCarrier-96 Ultra Microplates and infected with rRV-gs5*-HA-EGFP* at MOI of 5. After 1 hour, cells were stained with DAPI and live-cell imaging was started. Cells were imaged at 40x magnification (Olympus 40x NA 0.95) with a PerkinElmer Operetta High content microscope under controlled environmental conditions (37°C, 5% CO_2). Image acquisition was performed with intervals of 20 minutes for a total of 12 hours. Image were analyzed using Columbus analysis software (Perkinelmer) and total cell number, number of EGFP positive spots per cell and % of EGFP positive cells (number of NSP1-EGFP positive spots $\geq$ 1) were calculated for each time point at single cell level.

Sequencing of edited RV genomic segments

Extracted RNA was subjected to RT-PCR using NSP1-FOR and NSP1-REV primers for gs5* and gs5*HA. gs10* and gs7* were amplified using gs10*-FOR, gs10*-REV, gs7*-FOR, gs7*-REV respectively (Table S1). All primers contain HindIII and XhoI restriction enzyme sites at the 5′ and 3′ end, respectively. PCR products were either sequenced and analyzed using the TIDE software

(Brinkman et al., 2014) or gel purified before HindIII-XhoI digestion and cloning into pcDNA 3.1 plasmid. Colonies-derived PCR products were gel purified and sequenced.

PCR using splicing primers

Detection of specific edited RNAs, such as gs5*-Δ42 or gs5*-Δ27 was carried out by RT/PCR with primers gs5*-FOR and gs5*Δ42-REV or gs5*-FOR and gs5*Δ27-REV, respectively (Table S1). PCR amplification of gs5*-HA (213 bp) and gs5*-HA-Δ36 (177 bp) was performed using gs5*-HA-FOR and gs5*-HA-REV primers (Table S1). The latter allows specific amplification of only gs5*-HA and gs5*-HA-Δ36. PCR products were run on 2.5% agarose gel in TBE 1X (45 mM Tris-borate/1 mM EDTA) for 20 minutes at 120V. Quantification analysis of bands were carried out using ImageLab 6.0.1.

QUANTIFICATION AND STATISTICAL ANALYSIS

Statistical Analysis

Unless otherwise indicated, statistical analyses were performed with the Student's t test using GraphPad Prism 7 software (GraphPad). The number of experiments or (biological) replicates (n) used for the statistical evaluation of each experiment is indicated in the corresponding figure legends. The data are plotted as a mean ± SD or SEM as indicated.